

# Mixing through shear instabilities

M. Brüggen<sup>1,2</sup>, W. Hillebrandt<sup>1</sup>

<sup>1</sup> Max-Planck-Institut für Astrophysik, Karl-Schwarzschild-Str. 1, 85740 Garching, Germany

<sup>2</sup> Churchill College, Storey's Way, Cambridge, CB3 0DS, UK

19 November 2018

## ABSTRACT

In this paper we present the results of numerical simulations of the Kelvin-Helmholtz instability in a stratified shear layer. This shear instability is believed to be responsible for extra mixing in differentially rotating stellar interiors and is the prime candidate to explain the abundance anomalies observed in many rotating stars. All mixing prescriptions currently in use are based on phenomenological and heuristic estimates whose validity is often unclear. Using three-dimensional numerical simulations, we study the mixing efficiency as a function of the Richardson number and compare our results with some semi-analytical formalisms of mixing.

**Key words:** hydrodynamics, stars

## 1 INTRODUCTION

Mixing is a fundamental process which profoundly affects the evolution of stars. Nonetheless, a theory of mixing that is applicable to stellar conditions is still missing. Hitherto stellar evolution theory has resorted to more or less heuristic prescriptions of mixing, the validity of which is often unclear. One of the prominent mechanisms responsible for mixing in stars is the shear or Kelvin-Helmholtz instability. This instability is particularly important since most stars are known to be at least partly differentially rotating. Therefore, shear mixing is likely to play a significant role in stellar evolution.

Observational evidence seems to suggest that current prescriptions underestimate the efficiency of the mixing processes at work, especially in fast rotating stars. The observational evidence for mixing is increasing rapidly. Herrero et al. (1992) find that all fast rotating O-stars show significant surface He-enrichments. This seems to suggest that mixing is strong enough to transport the nuclearly processed material to the surface in a fraction of the life time of the star. Other observations include the N/C and <sup>13</sup>C and <sup>12</sup>C enrichments of the Red Giant Branch (e.g. Kraft 1997, Charbonnel 1995), the He and N excesses in OBA supergiants (Fransson et al. 1989), the depletion of boron in most B-type stars (Venn, Lambert & Lemke 1996) and the ratio of the number of blue to red supergiants in galaxies (Langer & Maeder 1995). For a more detailed review of the observational evidence see Maeder (1995), Kraft (1994) and references therein. But the conclusion from these observations is that both, the enrichment in CNO elements and the depletion of fragile elements such as boron can be explained if some form of mixing is

introduced (Langer 1997).

However, a convincing theory of mixing under most astrophysical conditions is still missing. One of the pioneering works in this field was performed by Endal & Sophia (1978) who estimated the efficiency of mixing due to several rotationally induced instabilities in massive stars.

The Sun is also known to rotate differentially. Pinsonneault et al. (1989) treated the efficiency of rotational mixing as a free parameter and fitted it to a solar model. In the meantime, helioseismological observations from the space-craft SOHO and from the GONG network have yielded precise measurements of the rotation rate in the solar interior. In a number of publications the effects of mixing on stellar evolution have been examined, see, e.g. Meynet & Maeder (1997) and Staritsin (1999). Recently, Denissenkov & Tout (2000) investigated the effects of 'deep mixing' on the evolution of red giants. However, for want of a valid fundamental theory, the mixing formalisms employed in the aforementioned studies have all been based on more or less heuristic estimates. It is the aim of this work to make steps towards a more fundamental theory of mixing.

In chemically homogeneous, stratified shear flows, the Kelvin-Helmholtz instability occurs when the destabilising effect of the relative motion in the different layers dominates over the stabilising effect of buoyancy (see e.g. Chandrasekhar 1961). The competition between the two effects is described by the Richardson number,  $Ri$ . For a non-dissipative, parallel, steady flow a simple linear stability criterion can be derived as follows: Let the horizontal velocity of the fluid be a function of  $z$  only, i.e.  $U = U(z)$ . Now suppose that two volumes of fluid at heights  $z$  and  $z + \Delta z$  are

interchanged where the densities at those two heights are  $\rho$  and  $\rho + \Delta\rho$ , and their horizontal velocities  $U$  and  $U + \Delta U$ , respectively. The work per unit mass that must be done against gravity is

$$\Delta W = -g\Delta\rho\Delta z. \quad (1)$$

After the exchange both cells have an average velocity of  $\bar{U} = \frac{1}{2}(2U + \Delta U)$ . Therefore, the kinetic energy available to do this work is

$$\frac{1}{2}\rho[U^2 + (U + \Delta U)^2 - \frac{1}{2}(2U + \Delta U)^2] = \frac{1}{4}\rho(\Delta U)^2. \quad (2)$$

Hence, a condition for stability is

$$\frac{1}{4}\rho(\Delta U)^2 < -g\Delta\rho\Delta z, \quad (3)$$

or

$$\left(\frac{dU}{dz}\right)^2 < -4\frac{g}{\rho}\frac{d\rho}{dz}. \quad (4)$$

A more general criterion can be derived (see e.g. Shu 1992):

$$\text{Ri} := \frac{N^2}{(dU/dz)^2} > \frac{1}{4}, \quad (5)$$

where  $N$  is the Brunt-Väisälä frequency given by

$$N^2 = \frac{g\delta}{H_P} \left[ \left( \frac{\partial \ln T}{\partial \ln P} \right)_{\text{ad}} - \frac{\partial \ln T}{\partial \ln P} + \frac{\phi}{\delta} \frac{\partial \ln \mu}{\partial \ln P} \right], \quad (6)$$

with  $\delta = -(\partial \ln \rho / \partial \ln T)_{P,\mu}$  and  $\phi = (\partial \ln \rho / \partial \ln \mu)_{P,T}$ , where  $T$  is temperature,  $P$  is pressure and  $\mu$  chemical potential.  $H_P$  is the pressure scale height, i.e.  $(\partial \ln P / \partial z)^{-1}$ .  $\text{Ri}$  is the so-called Richardson number. Stability is predicted if the *local* Richardson number exceeds 1/4 everywhere.

More detailed analytical theories of shear mixing have been developed (Maeder 1995, Canuto 1998) and some will be reviewed briefly in Sec. 2. In Sec. 3, we present the results of three-dimensional simulations of shear instabilities in stratified fluids. These numerical simulations were performed for a simple configuration and a range of initial condition. Our aim is to elucidate the nonlinear dynamics of the shear instability and to study the parametric dependence of the mixing efficiency on the Richardson number. We quantify the mixing of the fluid by introducing ‘tracer’ particles that are advected with the fluid. With conditions in stellar interiors in mind, we only consider subsonic flows. From the motion of these particles a heuristic diffusion constant can be derived which is then compared to the analytic prescriptions described in Sec. 2.

Apart from mixing by shear instabilities, there is another important candidate believed to be responsible for extra mixing in stars, namely convective overshoot. In models of stellar evolution the fluid is assumed to be mixed whereever some convective instability criterion (such as the Schwarzschild criterion) is fulfilled, and convectively stable where this criterion is not fulfilled. Mathematically the

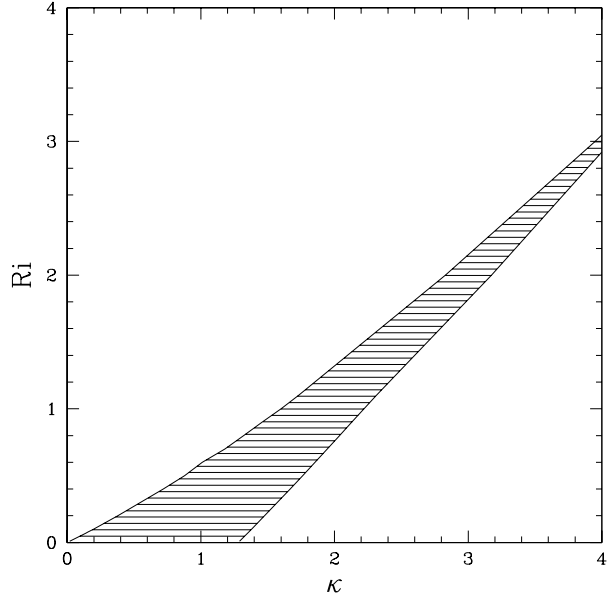


**Figure 1.** Region of instability (shaded) in the  $\kappa$ -Ri plane, where  $\kappa$  is the dimensionless wave number and Ri the Richardson number (see text).

boundary between these two regions is sharp. In reality, however, the convective fluid elements still carry some momentum when they reach this boundary and subsequently penetrate into the convectively “stable” region. This mechanism is called convective overshoot and has been investigated numerically by a number of groups (Freytag, Ludwig & Steffen 1996, Nordlund & Stein 1996, Singh, Roxburgh & Chan 1998) all of which find some degree of overshoot. This conclusion is supported by observations. The most compelling evidence stems from isochrone fitting to stellar clusters and binary systems which suggests that convective overshoot is significant (see Zahn 1991 for a review).

Unlike convective overshoot which provides mixing at the boundaries of convection zones, we investigate mixing by rotational instabilities that operate in convectively stable regions.

## 2 THEORIES OF SHEAR MIXING

### 2.1 Linear stability analysis of a shear layer

The stability of a stratified shear layer has been studied extensively using linear theory (see e.g. Chandrasekhar 1961, Howard & Maslowe 1973, Maslowe & Thompson 1971, Hazel 1972, Morris et al. 1990). Recently, Balmforth & Morrison (1998) reviewed the conditions for instability in inviscid shear flows. In astrophysics, Kippenhahn & Thomas (1987) and MacDonald (1983) examined the redistribution of matter and angular momentum in accreting white dwarfs by means of a linear stability analysis. In this section we will present a simple example of a linear stability analysis for a plane shear layer. The results of this analysis will then be compared against our numerical simulations in Sec. 3.

The stability equation for wave-like perturbations in

its inviscid and incompressible form can be written as (e.g. Chandrasekhar 1961)

$$\frac{d^2\phi}{dz^2} - \left( k^2 + \frac{U''}{U - c} - \frac{g\beta}{(U - c)^2} \right) \phi = 0, \quad (7)$$

where  $\beta = \rho'/\rho$  and  $\phi(z)\exp[ik(x - ct)]$  is the perturbation stream function. Eqn. (7) is sometimes referred to as the Orr-Sommerfeld equation. As an example for the linear analysis of the Kelvin-Helmholtz instability we will cite a case which was first considered by Taylor: It consists of two superposed fluids of different densities separated by a transition layer of intermediate density in which the shear velocity varies linearly from that of the lower layer to that of the upper layer, i.e.

layer 1:  $z > d$ ,  $\rho = \rho_0(1 - \epsilon)$ ,  $U = U_0$   
 layer 2:  $d > z > -d$ ,  $\rho = \rho_0$ ,  $U = U_0 z/d$   
 layer 3:  $z < -d$ ,  $\rho = \rho_0(1 + \epsilon)$ ,  $U = -U_0$ .

It is easily verified that the Richardson number for this problem is given by

$$Ri = \frac{g\epsilon d}{U_0^2}. \quad (8)$$

The solutions of eqn (7) in each of the three regions are

layer 1:  $\phi_1 = A_1 e^{-kz}$   
 layer 2:  $\phi_2 = A_2 e^{-kz} + B_2 e^{kz}$   
 layer 3:  $\phi_3 = A_3 e^{kz}$ .

Continuity of  $\phi$  at the interfaces, and requiring  $\phi$  to vanish at  $\pm\infty$ , gives the characteristic equation:

$$e^{-2\tilde{k}} = \left[ 1 - \frac{\tilde{k}(\tilde{c} + 1)^2}{Ri + (\tilde{c} + 1) + \frac{1}{2}\epsilon\tilde{k}(\tilde{c} + 1)^2} \right] \times \left[ 1 - \frac{\tilde{k}(\tilde{c} - 1)^2}{Ri - (\tilde{c} - 1) - \frac{1}{2}\epsilon\tilde{k}(\tilde{c} - 1)^2} \right], \quad (9)$$

where  $\tilde{k} = 2kd$  and  $\tilde{c} = c/U_0$ . Eqn (9) can now be solved numerically for  $c$  for a range of wave and Richardson numbers. When  $c$  becomes imaginary the perturbation becomes unstable. The parameter region in which this occurs, i.e. the region of instability, is shown in Fig. 1.

The efficiency of mixing is sometimes parametrized by a diffusion coefficient which can be loosely defined as

$$D(Ri) \sim \frac{\text{Im} [c_{\max}(Ri)]}{k_{\max}(Ri)}, \quad (10)$$

where  $\text{Im} [c_{\max}]$  is the maximal growth rate of the perturbations and  $k_{\max}$  the corresponding wave number - both evaluated at a given Richardson number. The diffusion coefficient as a function of the Richardson number is shown in Fig. 2. As expected,  $D$  rapidly decreases with increasing Richardson number.

In this section we presented an example of just one of the many instability analyses found in the literature. The example was chosen for its simplicity. Of course, more realistic velocity and density distributions have been studied since

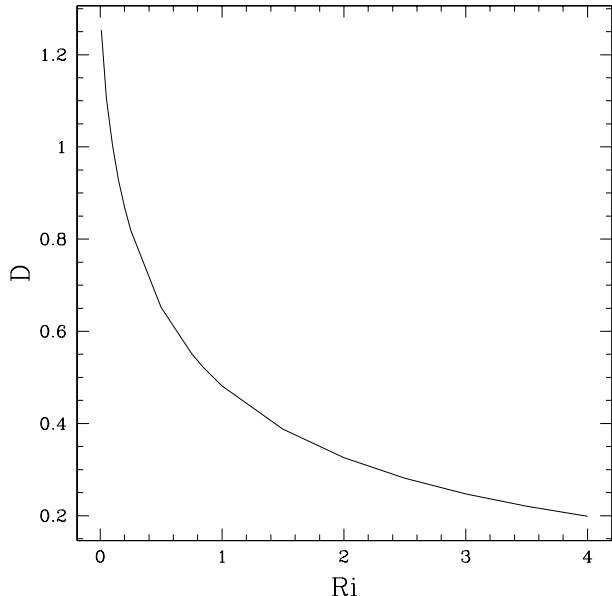


**Figure 2.** Diffusion coefficient (in units of  $U_0 d$ ) as a function of the Richardson number.

(see e.g. Chandrasekhar 1961, Howard & Maslowe 1973) but qualitatively they all yield the same picture as shown in Fig. 1. Linear stability analyses, however, are only valid for small perturbations. They can be useful for studying the onset of instability, but they are not very reliable in describing the form or the efficiency of mixing itself. This is a problem that requires numerical simulations and a set of such simulations will be presented below.

In the next subsection we will quote a thermodynamic estimate of the diffusion coefficient, before we move on to the numerical simulations in Sec. 3.

## 2.2 Maeder's prescription

Maeder (1995, 1997) reexamined the Richardson criterion taking into account radiative losses (also see Maeder & Zahn 1998). These authors derive a diffusion coefficient given by

$$D = K \frac{(dU/dz)^2}{N^2}, \quad (11)$$

where  $K$  is the thermal diffusivity  $K = 4acT^3/3\kappa\rho^2C_P$ ,  $a$  being the radiation density constant,  $c$  the speed of light,  $C_P$  the specific heat at constant pressure and  $\kappa$  the opacity. Maeder's prescription for mixing due to differential rotation has been used, e.g., by Langer (1992) and Denissenkov (1994) for evolutionary calculations for O and B stars in our Galaxy and the Large Magellanic Cloud. More recently, Denissenkov & Tout (2000) invoked a diffusion constant of the form of Eq. (11) to explain extra mixing in globular cluster red giants.

## 3 NUMERICAL SIMULATIONS

Here we present the results of numerical simulations of the dynamical shear instability in a stratified fluid. The simu-

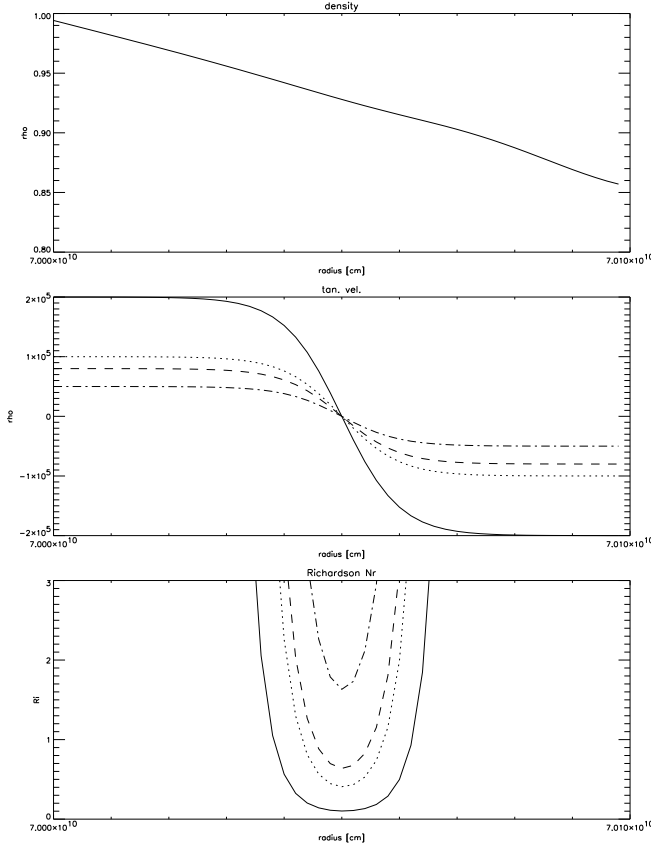


**Figure 3.** Top: Initial density stratification; Middle: Shear velocities for some selected simulations; Bottom: Corresponding Richardson numbers.

lations were obtained using the ZEUS-3D code which was developed especially for problems in astrophysical hydrodynamics (Clarke & Norman 1994). The code uses finite differencing on an Eulerian or pseudo-Lagrangian grid and is fully explicit in time. It is based on an operator-split scheme with piecewise linear functions for the fundamental variables. The fluid is advected through a mesh using the upwind, monotonic interpolation scheme of van Leer. For a detailed description of the algorithms and their numerical implementation see Stone & Norman (1992a, b).

In our simulations we employed an ideal gas equation of state, we ignored the effects of magnetic fields, rotation, nuclear reactions and variations in radiative processes. The simulations were computed on a Cartesian grid and the computational domain was chosen to have the dimension  $2 \cdot 10^8$  cm  $\times 2 \cdot 10^8$  cm  $\times 10^8$  cm (in the  $x$ -,  $y$ - and  $z$ -direction, where gravity acts in the  $z$ -direction). It was covered by  $100 \times 100 \times 50$  grid points. The calculations were performed on a CRAY Jedi parallel-processor and an IBM RS/6000 cluster.

The gravitational acceleration was taken to be that of a point mass of  $1 M_\odot$  at a distance of  $1 R_\odot$  from the lower boundary, where the gravitational acceleration acted purely in the  $z$ -direction. An analytic model for an isothermal density distribution under constant gravitational acceleration was relaxed in 1D until hydrostatic equilibrium was

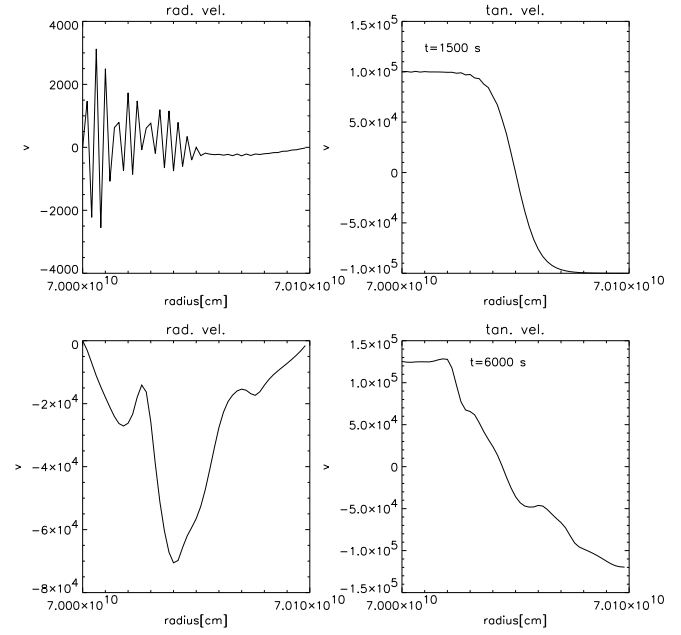


**Figure 4.** Radial and shear velocities at various times for the example with  $Ri=0.4$

attained. The residual velocities after the relaxation were six orders of magnitude smaller than the maximum shear velocities. The initial density distribution is shown in Fig. 3. Then a shear velocity profile was imposed on the fluid. It was chosen to have the form of a hyperbolic tangent in order to minimise the effect of the boundaries onto the shear layer, i.e.

$$U(z) = U_0 \tanh[(z - z_0)/h], \quad (12)$$

where  $U_0$  is the amplitude of the shear velocity,  $z$  the vertical position of the shear layer, and  $h$  its extent. In order to keep the shear layer away from the boundaries,  $h$  was taken to be smaller than the vertical extent of the simulation region. Finally,  $U_0$  was chosen to yield a range of initial Richardson numbers of 0.05 - 3, where the Richardson number is taken in its original simple definition, i.e.  $Ri = g\rho'/\rho U^2$ , and is measured at  $z = z_0$ . Fig. 3 shows the initial conditions for  $Ri = 0.1, 0.4, 0.6$  and  $1.6$ . The boundary conditions were chosen to be periodic in the  $x$  and  $y$  direction and reflecting in the  $z$  direction.

Figs. 4 and 5 show the  $x$ - and  $z$ -velocities in a vertical slice through the computational domain at various times, for a flow with an initial Richardson number of 0.4 in the shear layer. The occurrence of turbulence is clearly seen. One can see that early on in the simulation the flow undulates slightly before the instability becomes fully nonlinear. Then one can observe that two vortices form which mix material over a large section of the computational domain. The vortices remain quite stable and increase in size. Their centres coincide with the centre of the shear layer. One can also note that at the centre of the vortex, the flow velocity is very small. For efficient transport the velocity fluctuations in the horizontal and the vertical have to be correlated. This correlation is apparent in the formation of vortices as seen

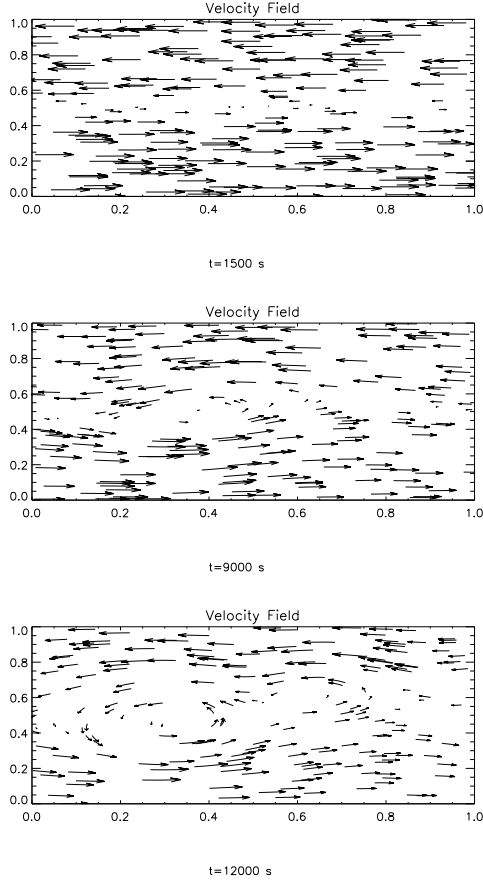


**Figure 5.** Velocity field at  $t = 1500$  s,  $t = 9000$  s and  $t = 12000$  s for the same case as shown in Fig. 4.

in Fig. 5. More quantitatively it can be expressed through the vorticity. Maps of the vorticity in the direction both perpendicular to the gravitational acceleration and the initial flow are shown in Fig. 6. (for  $Ri=0.4$ ). The contours in Fig. 6a. which show the vorticity after  $t = 1500$  s span a range of  $3 \cdot 10^{-3} \text{ s}^{-1}$  compared to a range of  $10^{-2} \text{ s}^{-1}$  in Fig. 6b. after 9000 s. This example shows the production of vorticity by the shear instability.

The eddies have the form of long ‘‘rolls’’ which are aligned with the  $y$ -axis, i.e. perpendicular to, both, the shear flow and the gravitational acceleration. They are found to stay fairly symmetric in the  $y$ -direction through the entire depth of the computational box. The structures on the big scales, as for example the ‘‘rolls’’ in our simulations, ‘feel’ the symmetry of the background model in the  $y$ -direction and therefore, they retain this symmetry. This has also been observed in laboratory experiments with incompressible fluids. Only on the small scales homogeneous, isotropic 3D turbulence will develop but we do not resolve these scales in our simulations. In the case of the shear instability, mixing is provided primarily by motions on big scales and, consequently, we argue that for our purpose we do not have to resolve these small scales. A further discussion of this issue can be found in Sec. 3.2.

Furthermore, over longer distances the ‘‘rolls’’ will start

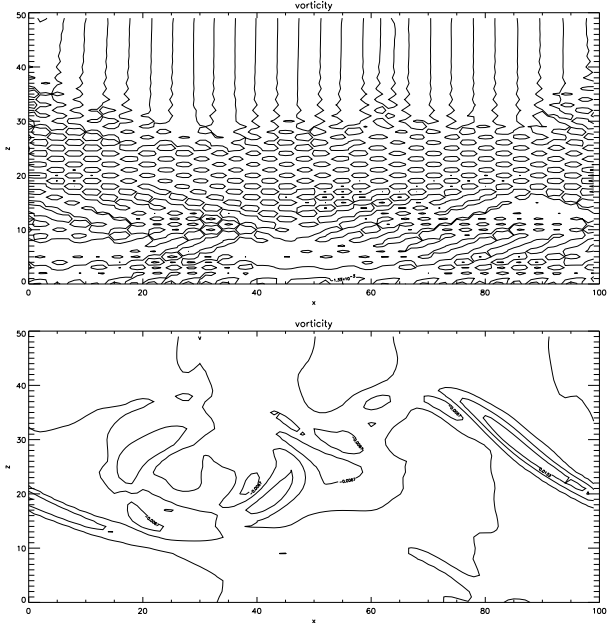


**Figure 6.** Vorticity after  $t = 4500$  s and  $t = 12000$  s for the example shown in Figs. 4. In the top panel the contours span a range in vorticity of  $3 \cdot 10^{-3} \text{ s}^{-1}$  and in the bottom panel a range of  $10^{-2} \text{ s}^{-1}$ .

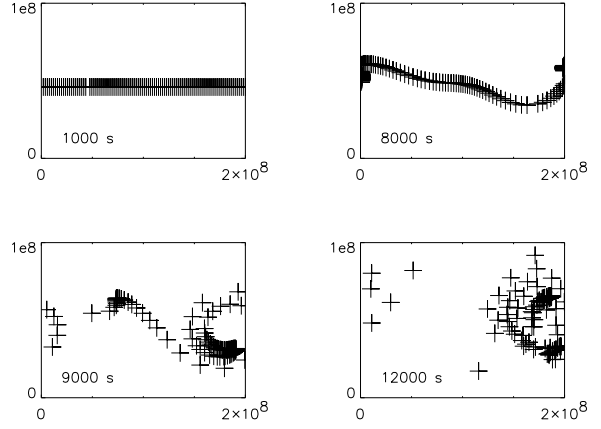


**Figure 7.** Positions of the tracer particles for the example shown in Figs. 4.

to feel the curvature of the star which is not accounted for in the slab geometry of our simulations and they may have the effect of breaking up the symmetry in the  $y$ -direction. These issues remain uncertainties in the results presented here and will have to be examined in a later study.

In order to study mixing processes the ZEUS code was modified to follow the motion of 1000 ‘tracer’ particles which are advected with the fluid. The positions of some of the tracer particles at various times (again for the case with  $Ri = 0.4$ ) are shown in Fig. 7.

The diffusion constant can then be defined as

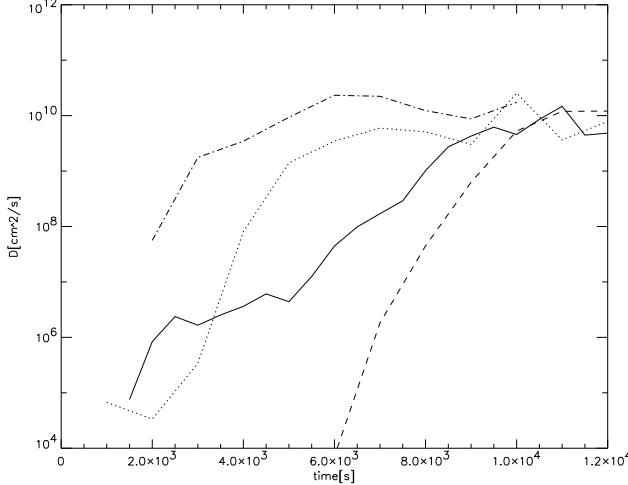


**Figure 8.** Diffusion coefficient as a function of time for  $Ri=0.4$ . The solid line shows the result of the 3D simulation and the dashed line the result of the 2D simulation with the same resolution. The dotted line represents the results from the computation on a  $200 \times 100$  grid and the dash-dotted line on a  $400 \times 200$  grid.

$$D = \sigma^2/t, \quad (13)$$

where  $\sigma^2 = \frac{1}{N} \sum_N [z(N) - z_0]^2$ ,  $z_0$  being the original height of the  $N$ th tracer particle and  $z(N)$  its height after a time  $t$ . As apparent from Fig. 7 the diffusion coefficient varies with time. The diffusion constant as a function of time have been plotted in Fig. 8. In Fig. 8 the Richardson number is 0.4, which is greater than 0.25 and, therefore, the flow should be stable to the shear instability according to the simple Richardson criterion. The simulations reveal that it is not, as has in fact been shown in previous simulations. One can observe that initially  $D$  rises with time before it eventually approaches a value which remains nearly constant for some time. The remaining scatter is mainly due to the stochastic nature of the turbulent mixing. The transient phase during which  $D$  rises is longer, the greater the Richardson number. Eventually, dissipation (mainly numerical) becomes noticeable and  $D$  starts to slowly decrease again. The constant value of  $D$  to which the curves are converging, is the value that is of greatest interest for the purpose of constructing stellar models. This value for  $D$  depends on the Richardson number. An understanding of the quantitative dependence of  $D$  on parameters such as the Richardson number will be useful for constructing stellar models which treat mixing through a diffusion equation.

We have plotted this ‘stationary’ value of  $D$  as a function of  $Ri$  for all the simulations which we have performed (see Fig. 10). The errorbars indicate the residual scatter observed in the simulations. Configurations with  $Ri > 1.6$  proved to be stable for times up to 30,000 s.

### 3.1 2D versus 3D simulations

Two-dimensional simulations of convective instabilities are known to introduce numerical artefacts and to yield unrealistic results. In 2D simulations of convection the energy

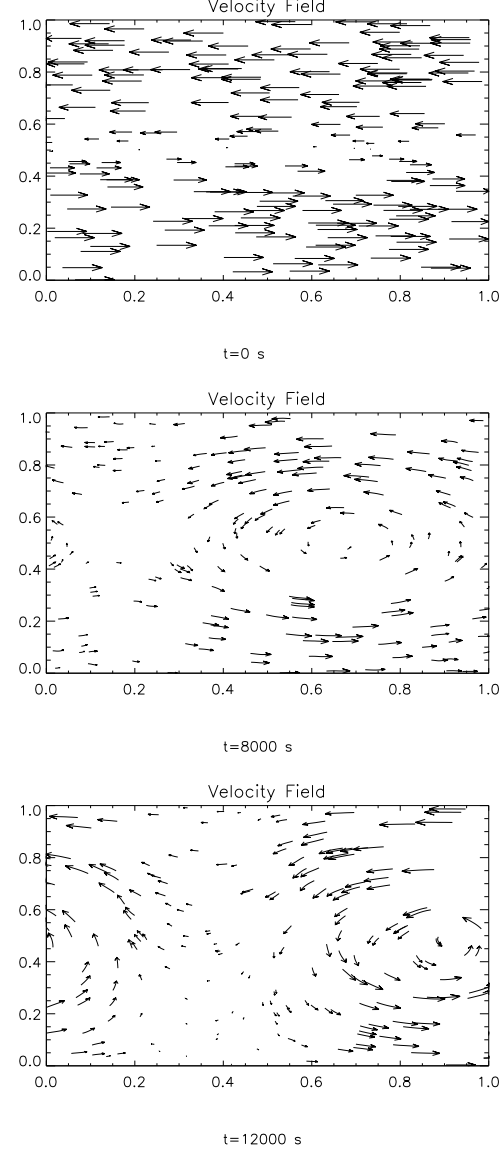


**Figure 9.** Velocity fields in a 2D simulation after  $t = 0$  s,  $t = 8000$  s and  $t = 12000$  s.

cascades to larger scales where viscous dissipation is less effective, whereas 3D simulations reveal that the energy cascades to smaller scales where it is absorbed. Moreover, 2D simulations often produce ‘rolls’, i.e. vortices in the direction perpendicular to the simulated domain, which, for convection, tend to overestimate the mixing.

In order to investigate the importance of performing these simulations in three dimensions, the runs described above were repeated in two dimensions. The ZEUS code is designed to efficiently compute on 1- and 2-dimensional grids, so the runs could be readily repeated in 2D. The same initial model and the same set of physical parameters as in the 3D simulations were used, and a grid of  $100 \times 50$  points was chosen. Fig. 9 shows a sequence of snapshots of the velocity.

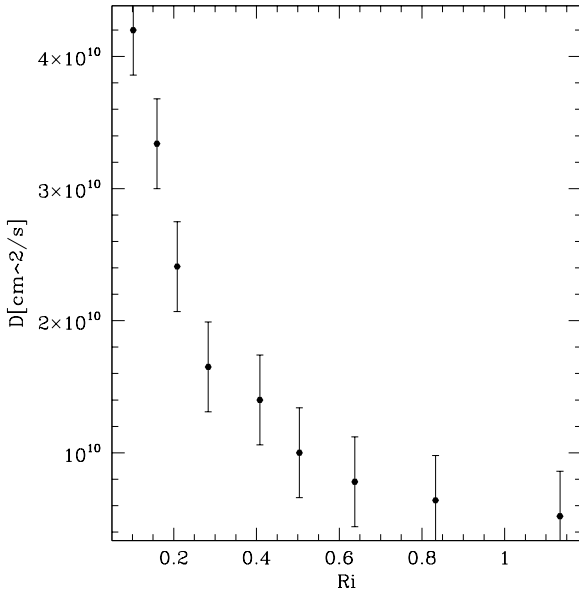


**Figure 10.** Diffusion coefficients for different Richardson numbers.

The diffusion coefficient derived from the 2D simulations as a function of time is displayed as a dashed line in Fig. 8. The figures show that in 2D simulations  $D$  rises more slowly with time than in three dimensions. But eventually  $D$  converges to about the same value which was obtained in the 3D simulations. This is an encouraging result. Not only does this raise the trust in the credibility and self-consistency of these results, it also suggests that 2D simulations may be sufficient to determine the efficiency of shear mixing. This conclusion may not be too surprising given that the 3D simulations revealed a flow structure consisting of long rolls that are parallel to the  $y$ -axis, i.e. perpendicular to the shear flow. On smaller scales, near the Kolmogoroff scale, the picture would look very different because one would observe the onset of full isotropic 3D turbulence. But here we are only simulating the Kelvin-Helmholtz instability and not full 3D turbulence which is a much more difficult problem and which requires a much finer (and yet unattained) numerical resolution. This will be discussed further in the next section.

### 3.2 Numerical viscosity

One frequently voiced objection to these kinds of direct numerical simulations is that Reynolds numbers as high as those encountered in stars are unattainable on current computers, and that therefore the results are unrealistic. But, as pointed out by Balbus, Hawley & Stone (1996), this criticism is unjustified for simulations of the shear instability. They argue, that in order to simulate the onset of instability in a laminar flow, it is merely necessary that the ‘typical’ wavelength of the instability is resolved by the numerical scheme and that the numerical diffusion at this wavelength is less than the growth rate. This makes the simulation of shear instabilities an easier task than the simulation of viscous instabilities where in theory one would have to resolve

everything down to the viscous length scale.

If the flow is unbounded, there is no viscous boundary layer which might interfere with the results. The nonlinear instabilities are fundamentally inviscid in character. Therefore, we only need a resolution capable of resolving a range of wavelengths with numerical diffusion errors less than the growth rates. This view is also supported by experimental observations which suggest that mixing through shear instabilities is dominated by large scale motions.

In Fig. 12 we have plotted the kinetic energy in the vertical ( $z$ -direction) as a function of time. The vertical kinetic energy is expressed in units of the total initial kinetic energy. In the beginning the energy is very small until the instability sets in. Then the kinetic energy jumps to about 10% of its total initial value and slowly decreases amidst big fluctuations. This decrease is mainly due to numerical viscosity and shows yet again that we are not simulating proper 3D turbulence which would show a saturation of the kinetic energy.

Porter & Woodward (1994) have estimated the Reynolds number of hydrodynamical simulations based on a PPM (piecewise parabolic method) code. The Reynolds number depends on the truncation error of the finite-difference algorithm, the Courant number, the background advection and the number of grid points. They found that the effective Reynolds number is proportional to the third power of the number of grid points, with the main dissipation occurring at short wavelengths. Above this critical wavelength the diffusion was found to be small. Since the ZEUS code uses piecewise linear functions instead of piecewise parabolic functions, the truncation errors of ZEUS will be larger than those of a PPM code. But even if they were only proportional to the second power of the number of grid points in one direction, we would still expect a numerical Reynolds number of around  $10^4$ .

The effect of the numerical viscosity is to suppress fluctuations beneath the ‘effective’ viscous length scale. This will become important for high enough Richardson numbers and all numerical simulations will find stability above a certain Richardson number. In our case the flow remained stable for  $Ri > 1.6$ . Higher resolutions, and therefore higher Reynolds numbers will push this limiting Richardson number to slightly higher values.

### 3.3 Dependence on grid size

We have investigated the dependence of our results on the resolution of the computational grid by repeating the 2D runs presented above ( $100 \times 50$ ) on grids with (b)  $200 \times 100$  and (c)  $400 \times 200$  grid points. The variation of  $D$  with time is shown in Fig. 8. by the dotted (b) and dash-dotted (c) lines. It is immediately evident that the behaviour of  $D$  with time varies with the numerical resolution. For more finely resolved grids,  $D$  rises more quickly. This was to be expected since higher resolutions produce higher Reynolds numbers and therefore a less viscous flow. For higher effective Reynolds numbers the turbulence grows more rapidly, and this is observed here. But again it merits mention that for all simulations  $D$  eventually converges to roughly the same

value for a given Richardson number, as long as the Richardson number is not too big. For large Richardson numbers, the numerical viscosity becomes important, but here we will restrict the discussion to Richardson numbers less than 2.

Finally, it can be seen in Fig. 5 that the eddies nearly span the entire vertical extent of the simulation domain. Hence, it is interesting to verify whether the vertical size of the computational domain affects the size of the eddies, and therewith the value of the mixing coefficients. We have repeated some 2D simulations in computational domains which had a vertical extent of more than  $50h$  or ten times the vertical size of the previously shown simulations. We did not find that the eddies became bigger when the size of the computational box was increased.

#### 4 DISCUSSION

In this paper results of direct numerical simulations of shear instabilities were presented. The simulations were carried out using the ZEUS hydro code. A chemically homogeneous stratified fluid in hydrostatic equilibrium was set up, onto which a shear flow was superimposed. The mixing was quantified by studying the dispersion of ‘tracer’ particles that are advected by the fluid. Thus, the variation of the diffusion constant with the Richardson number was examined.

In accordance with previous simulations, it was found that efficient mixing occurs for Richardson numbers substantially higher than 0.25, contrary to the simple linear stability criterion. Now the diffusion coefficients that were derived from the motion of the tracer particles can be compared to the analytical estimates discussed in Sec. 2. Applying Maeder’s formalism to our initial model, i.e. Eqn (11), yields substantially lower values for  $D$  than found in our simulations. For our initial models, Maeder’s diffusion coefficients in the centre of the shear layer lie between values of  $10^6$  -  $10^7$  cm<sup>2</sup>/s. This is more than 3 orders of magnitude smaller than the diffusion coefficients found here. Finally, one might want to compare our results with Fig. 2, even though this figure assumed a different shear velocity distribution than the hyperbolic tangens used in the simulations. In Fig. 11 where the dimensionless diffusion coefficient (in units of  $U_0h$ ) is plotted against the Richardson number. This dimensionless presentation is also useful for a wider application of our results. It is interesting to note that now our values for  $D$  are smaller by almost two orders of magnitude than those predicted by the linear analysis of our simple model of Sec. 2.

It was argued that numerical viscosity has no great effect on our findings as the effective Reynolds number is small on the scales on which the Kelvin-Helmholtz instability operates. This is true as long as the Richardson number is not too big. Furthermore, the differences between 2D and 3D simulations of shear instabilities were studied. We found that the dimensionality of the simulation hardly affects the final ‘steady state’ diffusion coefficient. It only affects the dynamics of the onset of the instability until a quasi-stationary state has been reached. The same qualitative observation was made when the resolution of the numerical grid was var-

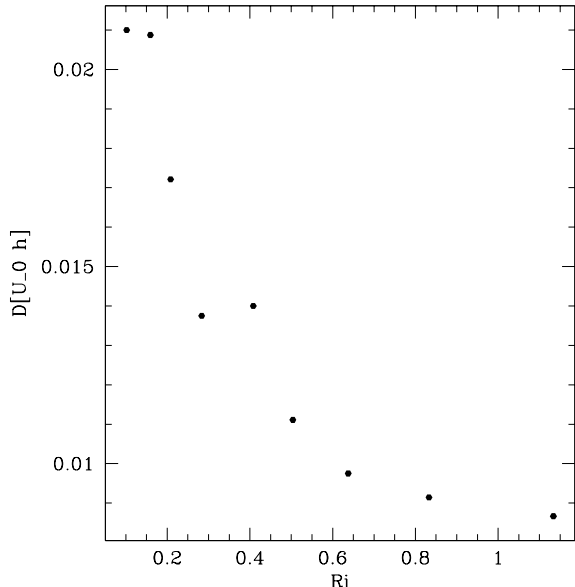


**Figure 11.** Diffusion coefficients for different Richardson numbers in units of  $U_0h$  (errorbars have been omitted).

ied. It was found that the resolution affects the initial temporal variation of the diffusion coefficient, but hardly affects the final value of  $D$ . However, the similarity between the 2D and 3D simulations is only valid on the big scales which we are resolving. On smaller scales, near the Kolmogoroff scale, one would observe full isotropic 3D turbulence which looks very different in two dimensions.

To make the Richardson number the only controlled parameter in our study, is clearly a simplification of the factors that determine the efficiency of mixing. In reality, the efficiency of mixing will depend on the density stratification and the velocity gradient separately, and not solely on the Richardson number. Moreover, the mixing will depend on the exact shape of the velocity profile and, only to a first approximation, on its first derivative. Nevertheless, if one is interested in the efficiency of mixing as a function of a single parameter, e.g. for stellar evolution studies, the Richardson number is still the most suitable parameter, since in the limit of an inviscid and incompressible shear flow, the stability is governed by the Richardson number.

In this work the effects of the dynamical shear instability in a plane shear layer were investigated. Clearly, this is not the only mechanism responsible for mixing in stars. In rotating fluid bodies other instabilities may occur, such as, e.g., the Solberg-Holand instability, the Eddington-Sweet instability and the Goldreich-Schubert-Fricke instability. However, the shear instability operates on the dynamical timescale whereas the instabilities tied to the rotation occur on the longer Eddington-Vogt timescale. Therefore, these instabilities operate on a much longer timescale and therefore play a lesser role in diffusion processes, even though they can affect the long-term evolution of the star.

The consequences of the newly found diffusion coeffi-

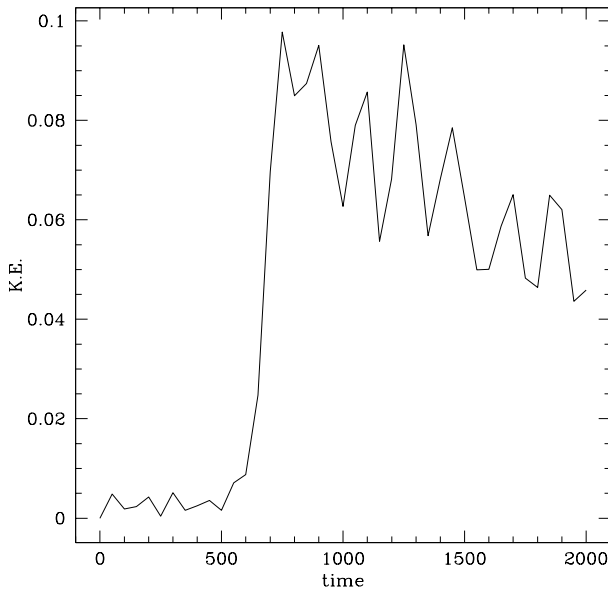


**Figure 12.** Kinetic energy in the vertical  $z$ -direction as a function of time. The kinetic energy is expressed in units of the total initial kinetic energy and the units of time are arbitrary.

clients onto stellar evolution and surface abundances are difficult to foresee. In stars the speed as well as the depth of mixing determine the balance between mixing and nuclear burning. Therefore, the effect of mixing depends sensitively on the conditions prevailing in the star, as for example the positions and extents of its convection and burning shells.

Finally we should mention that a number of factors can inhibit or facilitate mixing such as gradients in the chemical potential of the fluid, diffusion of radiation, magnetic fields and effects pertaining to the spherical geometry. In late-type stars strong chemical composition gradients exist, which will have a stabilising effect on the stratification. Therefore, especially for stellar evolution studies, the chemical composition gradient is an important parameter, which will have to be included in future work. Similarly, poloidal magnetic fields, as they are believed to exist in the Sun, will also suppress mixing processes. These effects are potentially of great importance in stars and will be studied in a forthcoming paper.

## ACKNOWLEDGEMENTS

A part of the simulations were performed on computers of the Rechenzentrum Garching. We thank Phil Armitage for helpful discussions and the referee for useful comments.

## REFERENCES

Balbus, S.A., Hawley, J.F., & Stone, J.M. 1996, *Astrophys. J.*, 467, 76  
 Balmforth, N.J., Morrison, P.J., 1998, *Studies in Applied Mathematics*, preprint no. physics/9809024  
 Chandrasekhar, S., 1961, *Hydrodynamic and Hydromagnetic Stability*, Clarendon Press, Oxford

Canuto, V.M., 1998, *Astrophys. J.*, 508, 767  
 Charbonnel, C. 1995, *Astrophys. J.*, 453, L41  
 Denissenkov, P.A. 1994, *A&A*, 287, 113  
 Denissenkov, P.A., Tout, C.A., 2000, *MNRAS* in press  
 Endal, A.S., Sofia, S. 1978, *Astrophys. J.*, 220, 279  
 Fransson, C. et al. 1989, *Astrophys. J.*, 336, 429  
 Freytag, B., Ludwig, H.-G., Steffen, M. 1996, *A&A*, 313, 497  
 Hazel, P. 1972, *J. Fluid Mech.*, 51, 39  
 Heger, A. 1996, *The Presupernova Evolution of Rotating Massive Stars*, PhD thesis, Max-Planck-Institut für Astrophysik, Garching  
 Herrero, A. et al., 1992, *A&A*, 261, 209  
 Howard, L.N., Maslowe, S.A. 1973, *Boundary-Layer Meteorology*, 4, 511  
 Kippenhahn, R., Thomas, H.-C., 1978, *A&A*, 63, 265  
 Kraft, R.P., 1994, *PASP* 106, 553  
 Kraft, R.P., Sneden, C., Smith, G.H., Shetrone, M.D., Langer, G.E., Pilachowski, C.A., 1997, *AJ* 113, 279  
 Langer, N., 1992, *A&A*, 265, L17  
 Langer, N., Maeder, A., 1995, *A&A*, 295, 685  
 MacDonald, J., 1983, *Astrophys. J.* 273, 289  
 Maeder, A., 1997, *A&A*, 321, 134  
 Maeder, A., 1995, *A&A*, 299, 84  
 Maeder, A., Zahn, J.-P., 1998, *A&A*, 334, 1000  
 Maslowe, S.A., Thompson, J.M., 1971, *Phys. Fluids* 14, 453  
 Meynet, G., Maeder, A., 1997, *A&A*, 321, 465  
 Morris, P.J., Giridharan, M.G., Lilley, G.M., 1990, *Proc. R. Soc. Lond. A*, 431, 219  
 Nordlund, A., Stein, R.F. 1996  
 Pinsonneault, M.H., et al., 1991, *Astrophys. J.*, 367, 239  
 Porter, D.H., Woodward, P.R., 1994, *ApJS*, 93, 309  
 Shu, F.H., *The Physics of Astrophysics Vol. II*, 1992, Univ. Science, Mill Valley  
 Singh, H. P., Roxburgh, I. W., Chan, K. L. 1998, *A&A*, 340, 178  
 Staritsin, E.I., 1999, *Astron. Rep.*, 43, 592  
 Stone, J.M., Norman, M.L., 1992a, *ApJS*, 80, 753  
 Stone, J.M., Norman, M.L., 1992b, *ApJS*, 80, 791  
 Venn, K.A., Lambert, D.L. & Lemke, M. 1996, *A&A*, 307, 894  
 Zahn, J.-P. 1991, *A&A*, 252, 179